CHEMISTRY
A EUROPEAN JOURNAL

FULL PAPER

DOI: 10.1002/chem.201300245

Dual-Mesoporous ZSM-5 Zeolite with Highly *b*-Axis-Oriented Large Mesopore Channels for the Production of Benzoin Ethyl Ether

Xiaoxia Zhou,[a] Hangrong Chen,*[a] Yan Zhu,[a] Yudian Song,[a] Yu Chen,[a] Yongxia Wang,[a] Yun Gong,[a] Guobin Zhang,[a] Zhu Shu,[a] Xiangzhi Cui,[a] Jinjin Zhao,[b] and Jianlin Shi*[a]

Abstract: Dual-mesoporous ZSM-5 zeolite with highly *b* axis oriented large mesopores was synthesized by using nonionic copolymer F127 and cationic surfactant CTAB as co-templates. The product contains two types of mesopores—smaller wormlike ones of 3.3 nm in size and highly oriented larger ones of 30–50 nm in diameter along the *b* axis—and both of them interpenetrate throughout the zeolite crystals and interconnect with zeolite microporosity. The dual-mesoporous zeolite exhibits excellent catalytic performance in the condensation of benzaldehyde with ethanol and greater than 99% selectivity for benzoin ethyl ether at room temperature, which can be ascribed to the zeolite lattice structure offering catalytically active sites and the hierarchical and oriented mesoporous structure providing fast access of reactants to these sites in the catalytic reaction. The excellent recyclability and high catalytic stability of the catalyst suggest prospective applications of such unique mesoporous zeolites in the chemical industry.

Keywords: heterogeneous catalysis · hydrothermal synthesis · mesoporous materials · template synthesis · zeolites

Introduction

Zeolite ZSM-5, a heterogeneous solid acid catalyst with MFI cages connected by 10-ring micropores, has been widely used in the fields of oil refining and petrochemistry.[1] However, the limited dimensions of the micropores not only strongly hinder the diffusion of large molecules, but can significantly slow down mass transport to and from active sites located within the micropores. This major drawback can strongly restrict its catalytic performance in various industrial reactions, for example, cracking, oxidation, alkylation, esterification, and isomerization.[2] Great efforts to overcome these problems have been made over the past years, such as the synthesis of nanosized zeolites,[3] large-pore zeolites,[4] and ordered mesoporous materials (e.g., MCM-41 and SBA-15).[5] However, up to now, the use of these materials is still limited owing to their inherent problems. For example, the difficulty of separating nanosized zeolite particles from a reaction mixture and the facile formation of aggregates of nanosized zeolites during synthesis and catalytic reactions would hinder practical applications of nanosized zeolites. The relatively low thermal stability of ordered mesoporous materials is also unfavorable for practical catalytic processes. Alternatively, the concept of hierarchically porous zeolites was proposed in recent years, and opens up a new mode of heterogeneous catalysts.[6] The successful fabrication of hierarchically porous zeolite can efficiently solve the problems associated with nanosized zeolites, large-pore zeolites, and mesoporous materials.[7] Hierarchically porous zeolites integrate at least two levels of porosity, that is, micro/mesopores and/or micro/meso/macropores.[8] However, the macropores (>50 nm) in zeolites contribute little to the surface area and will easily collapse during heat treatment. Therefore, hierarchically porous zeolites containing an interpenetrating micro/mesoporous system are more practical and favorable for efficient solid acid catalysts.

Many surfactants have been used as templates for creating inter/intracrystalline mesoporosity in zeolites. For example, Schuth et al. synthesized mesoporous silicalite-1 zeolite by using an organic aerogel as a "soft" template.[9] Xiao et al. prepared hierarchically structured zeolites templated by cationic polymers.[6b,10] Notably, these mesopores are randomly oriented in zeolite crystals, and the synthesis of hierarchically porous zeolite containing dual mesoporosity has not been reported yet. Therefore, the synthesis of dual-mesoporous zeolite ZSM-5 and control of mesopore orientation in zeolites continue to be a great challenge. It is believed that the

[a] Dr. X. Zhou, Prof. H. Chen, Dr. Y. Zhu, Y. Song, Dr. Y. Chen, Dr. Y. Wang, Dr. Y. Gong, Dr. G. Zhang, Dr. Z. Shu, Dr. X. Cui, Prof. J. Shi
State Key Laboratory of High Performance Ceramics and Superfine Microstructures, Shanghai Institute of Ceramics
Chinese Academy of Sciences, 1295 Ding-xi Road
Shanghai 200050 (P. R. China)
Fax: (+86) 21-5241-3122
E-mail: hrchen@mail.sic.ac.cn
jishi@mail.sic.ac.cn

[b] Dr. J. Zhao
School of Material Science and Engineering
Shijiazhuang Tiedao University
17 Northeast, Second Inner Ring, Shijiazhuang, Hebei (P. R. China)

Supporting information for this article is available on the WWW under http://dx.doi.org/10.1002/chem.201300245.

interconnected bimodal and/or oriented mesopore system can further facilitate the diffusion and transport of reactant/product molecules in catalytic reactions. In addition, it is still difficult to prepare mesoporous zeolite by using conventional amphiphilic copolymers as templates because of the weak interaction between the copolymers and silica species in basic media. Therefore, the real difficulty in the synthesis of oriented dual-mesoporous zeolites is to understand the assembly mechanism among different template molecules and silicon/aluminum sources, and how to achieve an elaborate balance between zeolite crystallization and mesoporous phase formation, so that crystallization/growth of zeolite particles can be controlled to a certain degree to match the assembly of the mesoporous phase.[11]

Benzoin ethyl ether has been widely applied as a photosensitizer in the printing and coating industries. In the traditional industrial production, benzoin ethyl ether is usually synthesized in a two-step process. First, benzoin is prepared by condensation of benzaldehyde under harsh reaction conditions. Second, benzoin ethyl ether is obtained by condensation of benzoin with ethanol, in which cyanide and vitamin B1 are usually employed as catalysts; the former is toxic and the later is not effective enough. Therefore, the rapid synthesis of large amount of benzoin ethyl ether is still a great challenge. Recently, it was reported that the benzoin ethyl ether could be obtained by a one-step process over an NiAl-LDHs/SiO_2 catalyst (LDH = layered double hydroxide),[12] but it needs an elevated reaction temperature (343 K) and complicated catalyst composition.

Herein, we report a facile route for the controlled synthesis of dual-mesoporous zeolite ZSM-5 with highly *b* axis oriented large mesopores (ZSM-5-ODM) by using conventional cationic cetyltrimethylammonium chloride (CTAB) and nonionic amphiphilic copolymer F127 as co-templates. Two types of mesopores are present throughout the whole zeolite crystals and form a highly interpenetrating and uniform porous network. Interestingly, the larger mesopores grow with a preferred orientation in the zeolite crystals. Zeolite ZSM-5-ODM not only provides free diffusion pathways for large molecules and thus fast access to active zeolite sites, but also shows high thermal stability owing to the well-crystallized framework. As a heterogeneous solid acid catalyst, ZSM-5-ODM exhibits excellent catalytic properties in the conversion of benzaldehyde with high selectivity for benzoin ethyl ether at room temperature. Moreover, the results of cycle tests on the catalyst demonstrate that the catalytically active sites can be regenerated by a simple calcination process.

Results and Discussion

Synthesis of dual-mesoporous zeolite ZSM-5 with highly *b* axis oriented large mesopores (ZSM-5-ODM): Zeolite ZSM-5-ODM was obtained by a progressive aggregation–assembly process (Scheme 1). Firstly, silicate and aluminate oligomers, generated by hydrolysis and condensation of tetraethoxysilane and aluminum isopropoxide, further condensed into primary aluminosilicate units (zeolite seeds) in alkaline solution (tetrapropylammonium hydroxide). Dynamic light scattering (DLS) was employed to roughly measure the sizes of the zeolite seeds in the precursor liquid (see Figure S1 in the Supporting Information). Zeolite seeds around 400 nm in size were found. Then, a solution of CTAB and F127 in ethanol/water was added in the aluminosilicate precursor solution. The hydrophilic ends of the positively charged CTAB micelles could bind to the hydrophilic and negatively charged zeolite seeds by both electrostatic in-

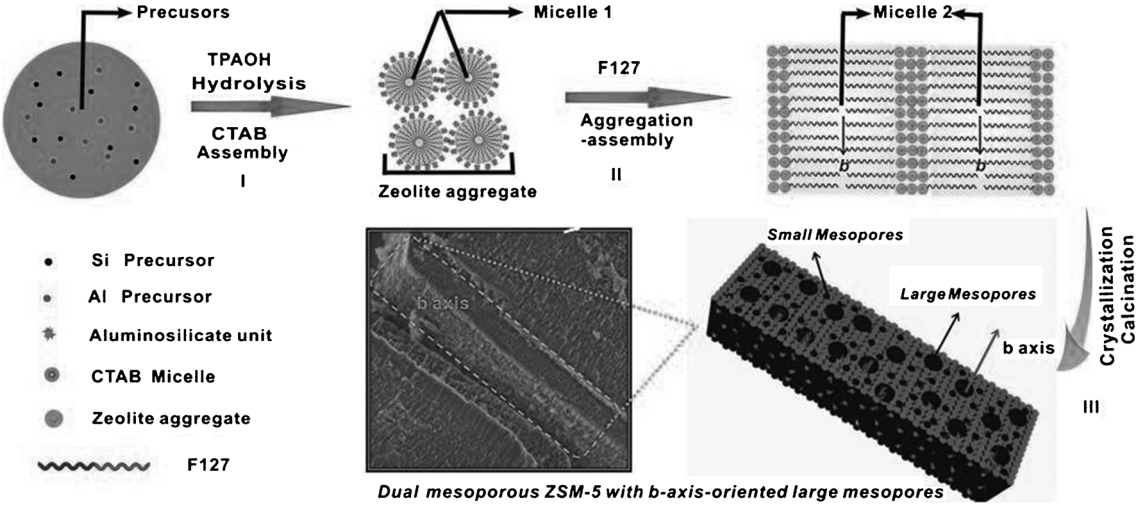

Scheme 1. Schematic of the formation mechanism of ZSM-5-ODM. Step I: Condensation between the primary aluminosilicates units (zeolite seeds) and CTAB micelles forming mesoporous zeolite aggregates. Step II: The zeolite aggregates stack along the *b* axis, and assembly between the aggregates and the F127 micelles leads to the synchronous formation of F127 micelles that are themselves *b*-axis-oriented in between the stacked aggregates. Step III: Further assembly, crystallization, and growth of the aggregates during hydrothermal treatment leading to the formation of dual-mesoporous ZSM-5 with *b*-axis-oriented large mesopores.

teraction and hydrophilic affinity on the surface of the seeds, and the seeds further condensed into mesoporous zeolite aggregates in the presence of attached CTAB micelles. Meanwhile, the concentration of the copolymer F127 significantly increases during the evaporation of ethanol, and these aggregates could assemble with the hydrophilic poly(ethylene oxide) (PEO) segments of triblock copolymer F127 by hydrogen bonding. Therefore, organic/inorganic composites with hydrophobic poly(propylene oxide) (PPO) cores and PEO/aluminosilicate aggregate shells assembled by a progressive aggregation–assembly process, and the hydrophilic PEO shell played an important role in stabilizing the large PPO/PEO/aluminosilicate aggregate micelles. According to ab initio DFT calculations, the (010) plane is the most favorable orientation among the (001), (010), and (101) planes of the zeolite ZSM-5 crystals for growth owing to the orientation and coordination of the exposed Si/O atoms on this particular plane.[13] Recently, Zhao et al. reported that additives can greatly impact the growth behavior of zeolite crystals to form aggregates of ZSM-5 nanorods.[14] We conjectured that the CTAB molecules, as organic additives with strong binding force to zeolite seeds, will first be adsorbed on the (010) plane and suppress the growth of ZSM-5 crystals along the *b* direction.[13] These additives can also act as linkers to form ZSM-5 aggregates which are crystallized to a certain extent and stack along the *b* axis, whereas the F127 micelles with weak binding activity can interact/bind with the *b*-axis-oriented stacked zeolite aggregates and themselves become *b*-axis-oriented. During the following hydrothermal treatment, these stacked zeolite aggregates and F127 micelles, both *b*-axis-aligned, further assemble with each other, crystallize, and simultaneously grow into large zeolite crystals with incorporated CTAB micelles and oriented F127 micelles. Finally, the templates were removed in a calcination process, leaving dual mesoporosity in the zeolite crystals. Thus, F127 and CTAB micelles are proposed to be templates for the large, oriented and small, wormlike mesoporosity, respectively. Moreover, the larger mesopores in ZSM-ODM aligned along the *b* axis are believed to result from aggregation–assembly of F127 micelles with large ZSM-5 aggregates.[8a]

The XRD pattern of ZSM-5-ODM (Figure 1a) shows well-resolved diffraction peaks of a typical MFI-type phase of zeolite ZSM-5. In addition, the small-angle XRD pattern of ZSM-5-ODM shows a clear signal at about 1.9°, which can be ascribed to the short-range ordered mesoporous structure. Figure 1b shows the N_2 adsorption/desorption isotherm and the corresponding pore size distribution curve of ZSM-5-ODM. The type IV adsorption/desorption isotherm with H1 hysteresis is indicative of the presence of a well-defined mesoporous structure. In particular, the sharp uptakes of nitrogen at relative pressures of $P/P_0 = 0.4$–0.5 and $P/P_0 = 0.90$–0.95 owing to capillary condensation inside the mesopores indicate the coexistence of two sets of mesopores in zeolite ZSM-5-ODM. The average pore size and pore volume of the smaller mesopores, calculated by means of the BJH adsorption model, are 3.3 nm and 0.12 $cm^3 g^{-1}$, and

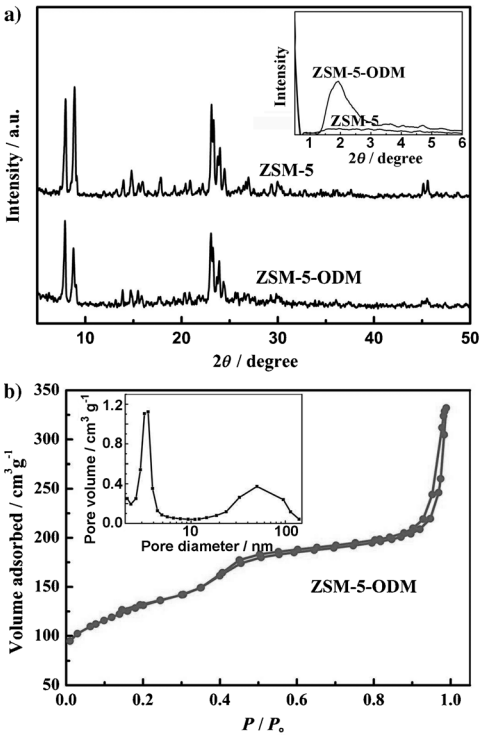

Figure 1. a) Small-angle and wide-angle XRD patterns of ZSM-5 and ZSM-5-ODM. b) N_2 adsorption/desorption isotherms and corresponding BJH pore diameter distribution curves of ZSM-5-ODM.

those of the larger mesopores are about 30–50 nm and 0.10 $cm^3 g^{-1}$, respectively. The BET surface area and total pore volume of ZSM-5-ODM are 487 $m^2 g^{-1}$ and 0.37 $cm^3 g^{-1}$, respectively. For comparison, the references ZSM-5-SM (single-mesoporous zeolite ZSM-5) with one type of mesoporous structure and a typical amorphous mesoporous material, namely, Al-MCM-41, were also synthesized (see Figure S2a,b in the Supporting Information). The BET surface area and total pore volume of ZSM-5-SM and Al-MCM-41 were calculated to be 597 $m^2 g^{-1}$, 0.57 $cm^3 g^{-1}$ and 859 $m^2 g^{-1}$, 0.82 $cm^3 g^{-1}$, respectively.

A low-magnification field-emission (FE) SEM image of ZSM-5-ODM (Figure 2a) reveals the presence of uniformly sized particles with similar interpenetrated morphology. The high-magnification FE-SEM images (Figure 2b and c) reveal the typical character of hierarchically porous zeolites, as was similarly observed in our previous reports.[11] The walls of the interpenetrated ZSM-5-ODM crystals have a porous structure. The larger mesopores (Figure 2c-d) of 30–50 nm in diameter are highly oriented in the direction of the *b* axis (as shown by arrows) and open only on the (010) plane, which is ascribed to the prior aggregation–assembly between amphiphilic F127 polymers and ZSM-5 aggregates along the *b* axis. The numerous wormlike smaller mesopores (ca. 3.3 nm in diameter, inset of Figure 2e) are distributed randomly in the whole zeolite crystals (Figure 2b and c). Compared with the single-mesoporous zeolite ZSM-SM, the dual-mesoporous zeolite ZSM-5-ODM with highly *b* axis oriented large mesopores more effectively favors the diffu-

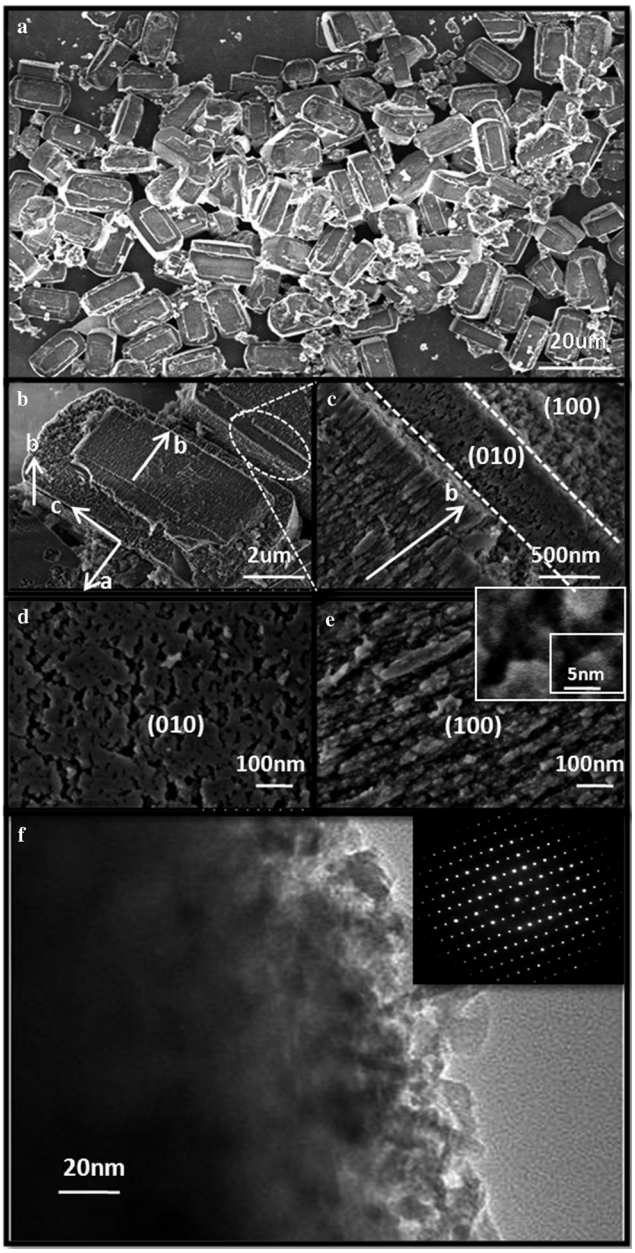

Figure 2. Low-magnification (a) and high-magnification (b, c) FE-SEM images of ZSM-5-ODM. d, e) FE-SEM images taken along the (010) and (100) planes of ZSM-5-ODM. The inset in e) is the a high-resolution image. f) Typical HRTEM image of ZSM-5-ODM and the corresponding SAED pattern (inset).

sion and transport of bulky reactant/product molecules. For comparison, the FE-SEM image of ZSM-5-SM (see Figure S3a in the Supporting Information) shows only one set of disordered wormlike small mesopores (ca. 3.2 nm).

A typical TEM image of ZSM-5-ODM confirms the presence of mesoporous and microporous structures (Figure 2 f). The random smaller mesopores can be seen in the figure, but larger mesopores are too large to be observed in the TEM image. In addition, ZSM-5-ODM shows clearly single-crystalline character, as indicated by the corresponding selected-area electron diffraction (SAED) pattern in Figure 2 f (inset), indicative of the coexistence of interpenetrating intrinsic microporosity and mesoporosity within zeolite particles. Compared with conventional mesoporous zeolites (see Figure S3b in the Supporting Information), the presence of the larger mesopores in the ZSM-5-ODM sample is believed to greatly favor mass transport of bulky molecules.

The Si/Al ratios of the synthesized samples ZSM-5, ZSM-5-SM, ZSM-5-ODM, and Al-MCM-41 of 50, 51, 46, and 48, respectively (Table 1), are similar to those of the precursor

Table 1. Texture properties, conversion of benzaldehyde, and selectivity for benzoin ethyl ether over various catalysts.[a]

Catalyst	Si/Al[b]	S_{BET} [$m^2 g^{-1}$]	V_{total} [$cm^3 g^{-1}$]	V_{meso} [$cm^3 g^{-1}$][c]	Conv. [%]	Select. [%]
ZSM-5	50	341	0.12	0.11	28.6	>99
ZSM-5-SM	51	597	0.57	0.49	47.4	>99
Al-MCM-41	46	859	0.82	0.80	62.0	76.4
ZSM-5-ODM	48	487	0.37	0.28	75.6	>99

[a] Catalytic properties were compared on the basis of the same weight of catalyst. All catalytic reactions were performed at room temperature. [b] Determined by ICP-AES analysis. [c] V_{meso} is given by the difference between V_{total} and the micropore volume.

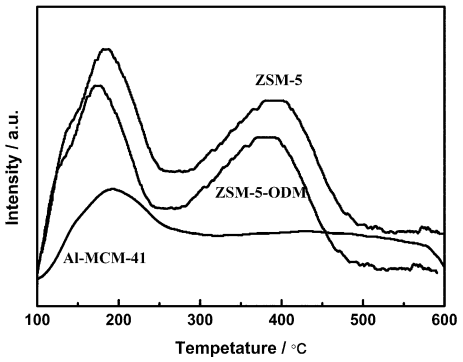

Figure 3. NH_3-TPD profiles of ZSM-5, ZSM-5-ODM, and Al-MCM-41.

solutions. The acidity of synthesized catalysts was studied by temperature-programmed desorption of ammonia (NH_3-TPD, Figure 3). Compared with ZSM-5 and ZSM-5-ODM, two distinct desorption peaks are present at about 180 and 400 °C, which can be attributed to the weak and strong acidic sites, respectively. The weak acidic sites are associated with the nonframework Al atoms and zeolite defects, while the strong acidic sites are related to the lattice Al atoms of the crystalline zeolite skeleton. Moreover, ZSM-5-ODM has a lower total acid content than the reference ZSM-5, owing to the introduction of mesoporous structure. Nevertheless, ZSM-5-ODM still retains the strong acidic sites of zeolite ZSM-5. Clearly, the mesoporous Al-MCM-41 sample has only weak acidic sites according to the NH_3-TPD profile around 200 °C, which can be due to the lack of lattice Al sites.

The structural configuration and the local environment of the Al and Si atoms were quantitatively analyzed by ^{27}Al

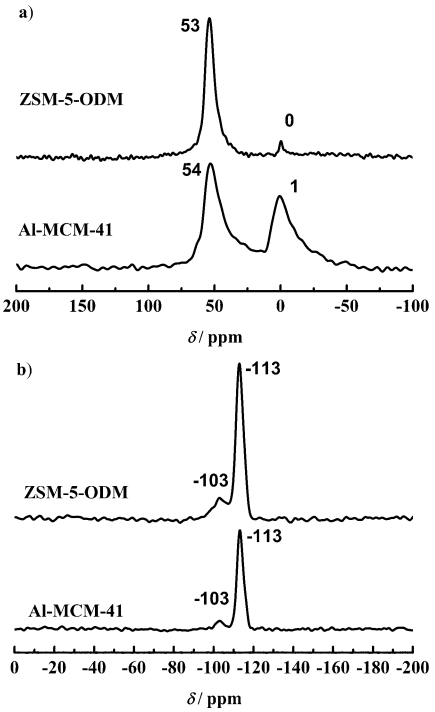

Figure 4. a) ^{27}Al and b) ^{29}Si MAS NMR spectra of ZSM-5-ODM and Al-MCM-41.

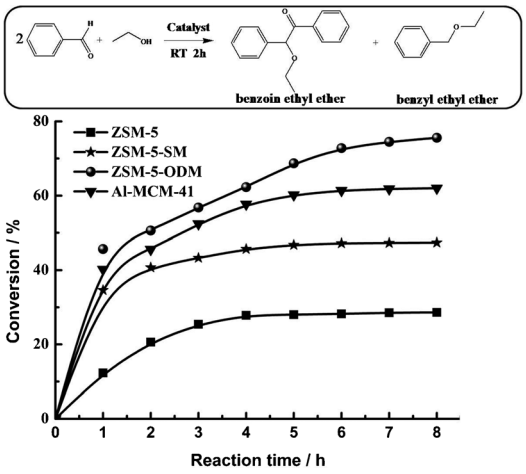

Figure 5. Condensation of benzaldehyde with ethanol and the effect of reaction time on the conversion of benzaldehyde over various catalysts.

and ^{29}Si MAS NMR spectroscopy (Figure 4). The ^{27}Al MAS NMR spectra of ZSM-5-ODM and Al-MCM-41 show characteristic peaks at about $\delta = 53$ ppm and $d = 54$ ppm, respectively, owing to tetrahedrally coordinated aluminum species. In addition, Al-MCM-41 exhibits a second peak at $\delta = 1$ ppm, which can be ascribed to octahedrally coordinated aluminum species. Interestingly, the ZSM-5-ODM only shows a weak peak at $d = 0$ ppm, which demonstrates that the Al atoms have been incorporated into the zeolite framework. The MAS ^{29}Si NMR spectra of ZSM-5-ODM and Al-MCM-41 clearly show two peaks with chemical shifts of $\delta = -103$ and -113 ppm, which are attributed to the (HO)Si-$(OSi)_3$ (Q3) and $Si(OSi)_4$ (Q4), respectively. The peak of ZSM-5-ODM at $\delta = -113$ ppm is stronger than that of Al-MCM-41, and the decrease in Q3/Q4 ratio indicates that the amorphous aluminosilicate walls were transformed into crystallized zeolite frameworks.[11b]

Catalytic properties of the dual-mesoporous zeolite ZSM-5-ODM, conventional zeolite ZSM-5, single-mesoporous zeolite ZSM-5-SM, and mesoporous material Al-MCM-41: Dual-mesoporous zeolite ZSM-5-ODM with highly *b* axis oriented large mesopores is expected to be applicable in many catalytic reactions. As a preliminary test, the condensation of benzaldehyde with ethanol was chosen as a model catalytic reaction. A series of differently synthesized catalysts were used in the conversion of benzaldehyde, and the results are summarized in Figure 5 and Table 1. Dual-mesoporous zeolite ZSM-5-ODM exhibits excellent catalytic properties compared with the conventional zeolite ZSM-5, single-mesoporous zeolite ZSM-5-SM, and mesoporous material Al-MCM-41 references in the condensation of benzaldehyde with ethanol at room temperature. The conversions of benzaldehyde increase steadily during the first 4 h over these catalysts, which can be ascribed to the presence of active acidic sites. However, beyond about 4 h, the conversions of benzaldehyde reach plateau values over ZSM-5, ZSM-5-SM, and Al-MCM-41 catalysts, which can most probably be attributed to blockage of pores by the produced bulky product molecules (e.g., benzoin ethyl ether) and coke formation in the smaller mesoporous channels of these catalysts during the prolonged reaction. In comparison, dual-mesoporous zeolite ZSM-5-ODM has significantly enhanced anti-coke-deposition performance due to the presence of larger oriented mesopores, which provide free diffusional access for the reactants/products, and the *b*-axis-aligned mesopores of the zeolite crystals are open to the surface and are accessible to bulky molecules.[8a] Hence, the conversion of benzaldehyde over ZSM-5-ODM continues to increase after 4 h.

Moreover, ZSM-5-ODM has the highest catalytic activity and selectivity to benzoin ethyl ether among the four catalysts (Table 1), giving benzaldehyde conversions of up to 75.6% and greater than 99% selectivity to benzoin ethyl ether after 8 h of reaction at room temperature. In contrast, the reference catalysts ZSM-5 and ZSM-5-SM show only 28.6 and 47.4% conversion, respectively, in the same reaction time. Although Al-MCM-41 shows a higher conversion of benzaldehyde (62.0%) than the other references, it has much lower selectivity to benzoin ethyl ether (76.4%) and a large amount of byproducts, such as benzyl ethyl ether, can be found in this reaction system. Thus, the large BET surface area and mesopore pore volume of Al-MCM-41 can accelerate the conversion of benzaldehyde, while the amorphous skeleton of Al-MCM-41 and the lack of strong acidic sites lead to the considerably lowered selectivity to benzoin ethyl ether. The above results suggest that both the acidic sites and mesoporous channels play an important role in the

conversion of benzaldehyde, and the strong acidity provided by crystalline zeolites makes a great contribution to high selectivity for benzoic ethyl ether. The large pore volume will lead to increased probability of reactants accessing active sites owing to the introduction of mesoporosity, which further enhances the conversion of benzaldehyde. Furthermore, the free access/diffusion of the reactants/products facilitated by dual mesoporosity, especially the oriented large mesopore channels, will effectively prevent catalyst deactivation due to greatly suppressed coke formation in the porous network, which frequently happens in microporous zeolites, especially when bulky molecules are involved. Therefore, the dual-mesoporous catalyst ZSM-5-ODM with highly *b* axis oriented large mesopores and crystalline zeolite framework exhibits much superior catalytic activity in the conversion of benzaldehyde compared to ZSM-5, ZSM-5-SM and Al-MCM-41.

More importantly, these catalysts could be well separated from the reaction solution by a filtration process. Unlike ZSM-SM and Al-MCM-41, the ZSM-ODM catalyst can be reused for four cycles with only slight loss of catalytic activity (Figure 6), which can be ascribed to the presence of

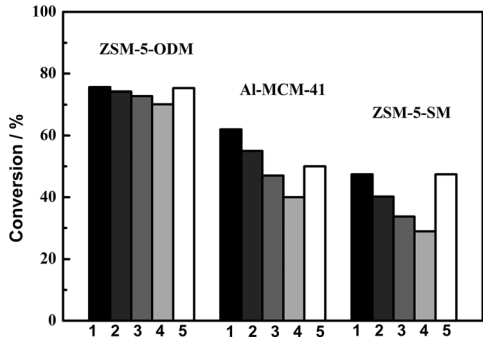

Figure 6. Recyclability of ZSM-5-ODM, Al-MCM-41, and ZSM-5-SM catalysts in the condensation of benzaldehyde with ethanol (1–4: the sample was recycled after separation by centrifugation from the product solution and reused in the conversion of benzaldehyde; 5: the sample was recycled after being calcined at 823 K for 8 h and reused in the conversion of benzaldehyde).

larger oriented mesopores. Interestingly, the catalytic activity of both ZSM-5-ODM and ZSM-SM can be almost fully recovered in the fifth cycle after a simple calcination treatment, while Al-MCM-41 shows much lower recyclability. This indicates that ZSM-5-ODM and ZSM-SM with crystalline frameworks have higher thermal stability than amorphous Al-MCM-41.

Conclusion

A novel aggregation–assembly process has been developed for the synthesis of the dual-mesoporous zeolite ZSM-5 with *b*-axis-aligned larger mesopore channels by using the nonionic copolymer F127 and the cationic surfactant CTAB as co-mesoporogens. Two types of interpenetrating mesoporosity are present throughout the whole zeolite crystals: smaller, wormlike mesopores of 3.3 nm in size and larger mesopores of 30–50 nm in diameter, which are highly oriented along the *b* axis of the zeolite crystals. The obtained catalyst shows excellent catalytic performance in the condensation of benzaldehyde with ethanol at room temperature, which can be ascribed to the free access of bulky reactants provided by the unique dual-mesoporous structure, especially the *b*-axis-oriented large mesopores, the large number of active sites, and the strong acidity offered by the crystalline structure of the zeolite framework. The catalyst can be reused and the catalytically active sites can be well regenerated by a simple calcination process. The oriented and dual-mesoporous zeolite is expected to be a highly efficient heterogeneous acid catalyst that can be applied in various chemical reactions involving bulky molecules.

Experimental Section

Dual-mesoporous zeolite ZSM-5 with highly *b* axis oriented large mesopores (ZSM-5-ODM): First, an emulsion containing of $Al(OiPr)_3$ (0.204 g) and of tetraethoxysilane (TEOS, 10.4 g) was stirred at 313 K for 30 min. Second, of tetrapropylammonium hydroxide (TPAOH, 4.06 g, 25 wt% solution) was added to the emulsion at 313 K, and the mixture was stirred at 313 K for a further 2 h. Subsequently, cetyltrimethylammonium chloride (CTAB, 1.53 g) and triblock copolymer $PEO_{106}PPO_{70}PEO_{106}$ (F127, 1.26 g) were dissolved in 20 mL of ethanol/water (1/9) to obtain a homogeneous solution, which was added to the reaction mixture at 313 K. Dual-mesoporous zeolite ZSM-5 was then obtained by hydrothermal treatment at 423 K for 16 h, after which the products were washed with distilled water and dried at 373 K. The final products were obtained after calcination at 823 K for 8 h to remove any organic substances (ZSM-5-ODM).

Zeolite ZSM-5: First, $Al(OiPr)_3$ (0.204 g) and TEOS (10.4 g) were dissolved in water (20 mL) to obtain a homogeneous solution at 313 K. Second, of TPAOH (4.06 g, 25 wt% solution) was added to the resultant solution at 313 K, and the mixture was stirred at 313 K for a further 6 h. Zeolite ZSM-5 was then obtained by hydrothermal treatment at 423 K for 16 h, after which the products were washed with distilled water and dried at 373 K. The final products were obtained after calcination at 823 K for 8 h to remove any organic substances.

Single-mesoporous zeolite ZSM-5 (ZSM-5-SM): First, an emulsion containing $Al(OiPr)_3$ (0.204 g) and TEOS (10.4 g) was added to distilled water (20 mL) and the mixture stirred at 313 K for 3 h. Second, TPAOH (4.06 g, 25 wt% solution) was added to the resultant solution, and the mixture was stirred and aged at 313 K for 6 h. Finally, the emulsion was added to solution of CTAB (1.53 g) in water (10 mL), and the reaction medium was stirred and aged at ambient temperature. ZSM-5-SM was then synthesized by hydrothermal treatment at 423 K for 16 h, after which the products were washed with distilled water and dried at 373 K. The final products were obtained after calcination at 823 K for 8 h to remove any organic substances.

Al-MCM-41: The synthesis of MCM-41 was carried out in a conventional hydrothermal system with a molar composition of $12NH_4OH:50SiO_2:0.5Al_2O_3:8.5CTAB:1200H_20$. First, $Al(OiPr)_3$ was dissolved in deionized water, and then ammonia hydroxide and CTAB were added to the solution. Second, TEOS was added to the mixture with strongly stirring. Mesoporous MCM-41 was then synthesized by hydrothermal treatment at 393 K and dried at 333 K. The final product were obtained after calcination at 823 K for 8 h.

Characterization: Powder XRD patterns were recorded on a Rigaku D/Max 2200PC diffractometer with $Cu_{K\alpha}$ radiation (40 kV and 40 mA) at a

scanning rate of 4° min^{-1} for high-angle measurements, and 0.4° min^{-1} for small-angle measurements. The nitrogen sorption measurements were performed with Micromeritics Tristar 3000 and Micromeritics ASAP 2020 porosimeters at 77 K; the mesoporous specific surface area and the pore size distribution were calculated by using the BET and BJH methods, respectively, while the micropore volume was calculated by the t-plot method. TEM imaging and SAED were performed on a JEOL-2010F electron microscope operated at 200 kV, and FE-SEM images were obtained on Hitachi S-4800. The acidic property of the zeolites were determined by temperature-programmed desorption of ammonia (NH_3-TPD). The Si/Al ratios were measured by inductively coupled plasma atomic emission spectroscopy (ICP-AES) on a Vista AX instrument. The particle size distribution of the mesoporous zeolite precursor was characterized by dynamic light scattering (DLS). ^{27}Al and ^{29}Si MAS NMR measurements were performed on Bruker DMX500 and Bruker DSX300 spectrometers, respectively.

Catalytic condensation of benzaldehyde with ethanol: All samples used in catalytic tests were in the H-form. In a typical run, the sample was ion-exchanged with 1 M NH_4NO_3 at 80 °C, and this procedure was repeated three times and followed by calcination at 500 °C for 3 h. The condensation reaction was conducted in a 50 mL three-necked flask equipped with a reflux condenser under stirred conditions. In a typical catalytic reaction, 100 mg of catalyst, 10 mmol of cyclohexane, and 10 mL of CH_3CH_2OH were mixed under continuous stirring. The mixture was stirred for a few minutes and the reaction was conducted at 298 K for 8 h. Benzyl chloride (1 g) was used as internal standard. The products were identified and analyzed by GC-MS (Agilent, 6890/5973N). After each benzaldehyde oxidation run, the catalyst was separated by centrifugation from the product solution, and reused for the next run under the same conditions.

Acknowledgements

This research was sponsored by National Key Basic Research Program of China (2013CB933200), China National Funds for Distinguished Young Scientists (51225202), National Natural Science Foundation of China (51202278, 51102172), Key Program for Science and Technology Commission of Shanghai Municipality (11JC1413400), State Key Laboratory of Heavy Oil Processing (2012-1-04), and Natural Science Foundation of Shanghai (12ZR1435).

[1] a) A. Corma, *J. Catal.* **2003**, *216*, 298–312; b) Y. Ni, A. Sun, X. Wu, G. Hai, J. Hu, T. Li, G. Li, *Microporous Mesoporous Mater.* **2011**, *143*, 435–442.

[2] a) J. Jiang, J. Yu, A. Corma, *Angew. Chem.* **2010**, *122*, 3186–3212; *Angew. Chem. Int. Ed.* **2010**, *49*, 3120–3145; b) C. Kresge, M. Leonowicz, W. Roth, J. Vartuli, J. Beck, *Nature* **1992**, *359*, 710–712.

[3] I. Schmidt, C. Madsen, C. J. H. Jacobsen, *Inorg. Chem.* **2000**, *39*, 2279–2283.

[4] J. Jiang, J. L. Jorda, J. Yu, L. A. Baumes, E. Mugnaioli, M. J. Diaz-Cabanas, U. Kolb, A. Corma, *Science* **2011**, *333*, 1131–1134.

[5] a) D. Zhao, J. Sun, Q. Li, G. D. Stucky, *Chem. Mater.* **2000**, *12*, 275–279; b) D. Margolese, J. Melero, S. Christiansen, B. Chmelka, G. Stucky, *Chem. Mater.* **2000**, *12*, 2448–2459.

[6] a) J. Aguado, D. Serrano, J. Rodriguez, *Microporous Mesoporous Mater.* **2008**, *115*, 504–513; b) F. S. Xiao, L. Wang, C. Yin, K. Lin, Y. Di, J. Li, R. Xu, D. S. Su, R. Schlögl, T. Yokoi, *Angew. Chem.* **2006**, *118*, 3162–3165; *Angew. Chem. Int. Ed.* **2006**, *45*, 3090–3093; c) J. C. Groen, W. Zhu, S. Brouwer, S. J. Huynink, F. Kapteijn, J. A. Moulijn, J. Pérez-Ramírez, *J. Am. Chem. Soc.* **2007**, *129*, 355–360; d) Z. Yang, Y. Xia, R. Mokaya, *Adv. Mater.* **2004**, *16*, 727–732; e) L. H. Chen, X. Y. Li, G. Tian, Y. Li, J. C. Rooke, G. S. Zhu, S. L. Qiu, X. Y. Yang, B. L. Su, *Angew. Chem.* **2011**, *123*, 11352–11357; *Angew. Chem. Int. Ed.* **2011**, *50*, 11156–11161.

[7] Z. L. Hua, J. Zhou, J. L. Shi, *Chem. Commun.* **2011**, *47*, 10536–10539.

[8] a) F. Liu, T. Willhammar, L. Wang, L. Zhu, Q. Sun, X. Meng, W. Carrillo-Cabrera, X. Zou, F. S. Xiao, *J. Am. Chem. Soc.* **2012**, *134*, 4557–4560; b) K. Moller, B. Yilmaz, R. M. Jacubinas, U. Muller, T. Bein, *J. Am. Chem. Soc.* **2011**, *133*, 5284–5295; c) S. Lopez-Orozco, A. Inayat, A. Schwab, T. Selvam, W. Schwieger, *Adv. Mater.* **2011**, *23*, 2602–2615; d) L. H. Chen, X. Y. Li, G. Tian, Y. Li, J. C. Rooke, G. S. Zhu, S. L. Qiu, X. Y. Yang, B. L. Su, *Angew. Chem.* **2011**, *123*, 11352–11357; *Angew. Chem. Int. Ed.* **2011**, *50*, 11156–11161.

[9] a) W. C. Li, A. H. Lu, R. Palkovits, W. Schmidt, B. Spliethoff, F. Schüth, *J. Am. Chem. Soc.* **2005**, *127*, 12595–12600; b) A. B. Laursen, K. T. Højholt, L. F. Lundegaard, S. B. Simonsen, S. Helveg, F. Schüth, M. Paul, J. D. Grunwaldt, S. Kegnæs, C. H. Christensen, *Angew. Chem.* **2010**, *122*, 3582–3585.

[10] X. Meng, F. Nawaz, F. Xiao, *Nano Today* **2009**, *4*, 292–301.

[11] a) Y. Zhu, Z. Hua, J. Zhou, L. Wang, J. Zhao, Y. Gong, W. Wu, M. Ruan, J. Shi, *Chem. Eur. J.* **2011**, *17*, 14618–14627; b) J. Zhou, Z. Hua, J. Shi, Q. He, L. Guo, M. Ruan, *Chem. Eur. J.* **2009**, *15*, 12949–12954.

[12] G. Wang, X. Xie, C. Gao, X. Wu, X. An, S. Cheng, *Chin. J. Inorg. Chem.* **2011**, *27*, 917–922.

[13] Z. Shan, H. Wang, X. Meng, S. Liu, L. Wang, C. Wang, F. Li, J. Lewis, F. Xiao, *Chem. Commun.* **2011**, *47*, 1048–1051.

[14] B. Li, B. Sun, X. Qian, W. Li, Z, Wu, Z. Sun, M. Qiao, M. Duke, D. Zhao, *J. Am. Chem. Soc.* **2013**, DOI: 10.1021/ja309194z.

Received: January 23, 2013
Published online: June 17, 2013

